

# Influence of the NO/NO<sub>2</sub> Ratio on Oxidation Product Distributions under High-NO Conditions

Kevin J. Nihill,\* Qing Ye, Francesca Majluf, Jordan E. Krechmer, Manjula R. Canagaratna, and Jesse H. Kroll

Cite This: *Environ. Sci. Technol.* 2021, 55, 6594–6601

Read Online

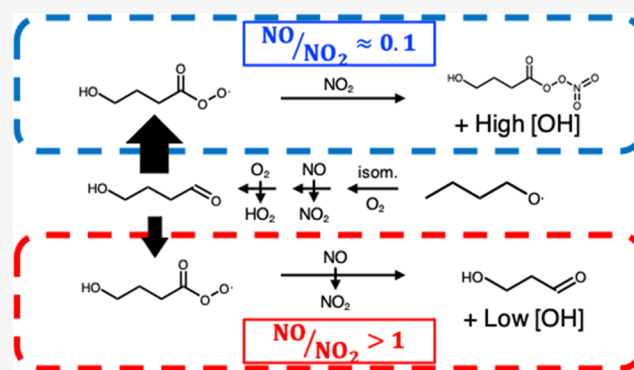
ACCESS |

Metrics & More

Article Recommendations

Supporting Information

**ABSTRACT:** Organic oxidation reactions in the atmosphere can be challenging to parse due to the large number of branching points within each molecule's reaction mechanism. This complexity can complicate the attribution of observed effects to a particular chemical pathway. In this study, we simplify the chemistry of atmospherically relevant systems, and particularly the role of NO<sub>x</sub>, by generating individual alkoxy radicals via alkyl nitrite photolysis (to limit the number of accessible reaction pathways) and measuring their product distributions under different NO/NO<sub>2</sub> ratios. Known concentrations of NO in the classically "high-NO" range are maintained in the chamber, thereby constraining first-generation RO<sub>2</sub> (peroxy radicals) to react nearly exclusively with NO. Products are measured in both the gas phase (with a proton-transfer reaction mass spectrometer) and the particle phase (with an aerosol mass spectrometer). We observe substantial differences in measured products under varying NO/NO<sub>2</sub> ratios (from ~0.1 to >1); along with modeling simulations using the Master Chemical Mechanism (MCM), these results suggest indirect effects of NO<sub>x</sub> chemistry beyond the commonly cited RO<sub>2</sub> + NO reaction. Specifically, lower-NO/NO<sub>2</sub> ratios foster higher concentrations of secondary OH, higher concentrations of peroxyacyl nitrates (PAN, an atmospheric reservoir species), and a more highly oxidized product distribution that results in more secondary organic aerosol (SOA). The impact of NO<sub>x</sub> concentration beyond simple RO<sub>2</sub> branching must be considered when planning laboratory oxidation experiments and applying their results to atmospheric conditions.



## INTRODUCTION

Atmospheric organic oxidation mechanisms are highly complex, involving numerous reaction branching points and multiple generations of oxidation for an individual compound.<sup>1,2</sup> The large number of products formed from a given compound, which is a strong function of the compound's structure and of reaction conditions, poses substantial challenges for the elucidation of detailed mechanisms and the prediction of major secondary species such as ozone and secondary organic aerosol (SOA).<sup>3–5</sup>

A key branch point in atmospheric oxidation mechanisms involves organic peroxy (RO<sub>2</sub>) radicals, which can react bimolecularly with NO<sub>x</sub>, HO<sub>2</sub>, or other RO<sub>2</sub> or undergo unimolecular reactions.<sup>5,6</sup> The role of NO<sub>x</sub> in the RO<sub>2</sub> fate is of particular interest as NO<sub>x</sub> is present across a wide range of concentrations in the atmosphere, varying from ppt levels in remote regions<sup>7</sup> to tens or even hundreds of ppb in urban settings and in biomass burning plumes.<sup>8–11</sup> Under high-NO concentrations (i.e., NO mixing ratios in the ppb level or higher), the dominant reaction pathway for peroxy radicals is RO<sub>2</sub> + NO → RO + NO<sub>2</sub>,<sup>4,5,12–15</sup> with a minor contribution from the reaction RO<sub>2</sub> + NO → RONO<sub>2</sub>.<sup>16–18</sup> Recent work on

NO<sub>x</sub> has gone beyond absolute NO<sub>x</sub> levels to focus on the role of the NO/NO<sub>2</sub> ratio in reaction mixtures. While some studies have explored the role of this ratio in terms of important subsets of atmospheric mechanisms (e.g., SOA, highly oxidized molecules),<sup>19–21</sup> the NO/NO<sub>2</sub> ratio has not been investigated in terms of its effects on the overall product distribution. This limits our ability to accurately predict how reaction systems respond to changes in NO<sub>x</sub> levels and risks leading to inaccurate recreations of "polluted conditions" in laboratory studies.

Here, we seek to better understand the detailed role of NO<sub>x</sub> and specifically the NO/NO<sub>2</sub> ratio, in influencing product distributions; this requires a reaction scheme in which the initiating chemistry is independent of NO<sub>x</sub> and the product distribution has a manageable complexity. We accomplish this

Received: November 10, 2020

Revised: April 8, 2021

Accepted: April 13, 2021

Published: April 26, 2021



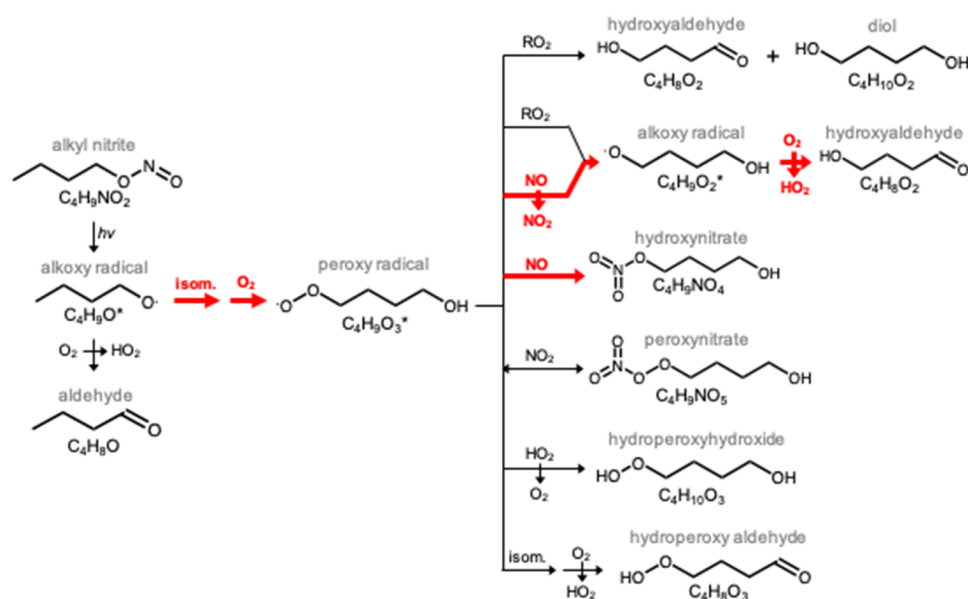


**Figure 1.** Major first-generation products of the photolysis of *n*-butyl nitrite. The resulting alkoxy radical will primarily isomerize, yielding an RO<sub>2</sub> radical that can undergo a number of different reactions. Red arrows indicate dominant reaction pathways under the high-NO conditions employed herein.

via the photolysis of alkyl nitrite (RONO) compounds<sup>22,23</sup> to directly generate alkoxy radicals (key intermediates in organic oxidation) in the presence of known concentrations of NO. For larger RO radicals, such as the *n*-butoxy radical shown in Figure 1, the dominant channel is isomerization to form an RO<sub>2</sub> radical, which can subsequently undergo a number of reactions. This method involves no direct introduction of gas-phase oxidants and the generation of a single initial organic radical (as opposed to a mixture of radicals arising from multiple potential OH-reaction sites, which is typical for oxidant-initiated chemistry), greatly simplifying the product distribution compared to traditional laboratory oxidation studies.<sup>22–24</sup> Moreover, it enables control over NO<sub>x</sub> levels in a manner that does not affect the initial reaction rate, thus facilitating the role of NO<sub>x</sub> to be studied directly.

These experiments are run under two NO concentrations, both within the classical “high-NO” limit ( $[\text{NO}] \gg 1$  ppb), but representing NO/NO<sub>2</sub> ratios that differ by over an order of magnitude. Such high concentrations of NO ensure that the initially formed RO<sub>2</sub> reacts almost exclusively with NO, thus making it possible to probe these simple RO<sub>2</sub> systems as a function of changing the NO/NO<sub>2</sub> ratio. Such systems can provide insight into the mechanisms underlying the NO<sub>x</sub>-dependence of VOC oxidation chemistry, specifically elucidating the role of the NO/NO<sub>2</sub> ratio in environmental chamber studies; this in turn may help to foster more realistic NO<sub>x</sub> conditions in chamber studies simulating the formation of SOA and other products under high-NO<sub>x</sub> reaction conditions.

## MATERIALS AND METHODS

**Chamber Conditions.** Reactions were carried out in a 150 L PFA chamber (described in detail elsewhere<sup>25</sup>) surrounded by an array of twelve 340 nm UV lights (Q-lab). The spectral distribution of these lamps overlaps well with the absorption spectrum of precursor RONO compounds,<sup>26</sup> ensuring rapid photolysis. UV irradiation in this wavelength range (290–400 nm) involves relatively low-energy photons, limiting the extent of vibrationally/electronically excited products.<sup>22,26</sup>

Experiments were run at room temperature ( $\sim 25$  °C) and pressure ( $\sim 1$  atm) in a semibatch mode, with sampling flows balanced by an equal input of pure, low-RH (<1%) air, resulting in a chamber residence time of approximately 15 min. Prior to each experiment, the chamber was flushed with pure, dry air for at least 1 h. Additionally, the internal walls of the chamber were cleaned between groups of experiments by flooding with O<sub>3</sub> and H<sub>2</sub>O while irradiating overnight.

Experiments were run under one of two NO concentrations to ensure the dominance of the RO<sub>2</sub> + NO reaction. In “higher-NO” experiments (NO/NO<sub>2</sub> > 1), the chamber was maintained at a constant concentration of  $\sim 1$  ppm NO by the continual addition of NO prior to and throughout the run. In “lower-NO” experiments (NO/NO<sub>2</sub>  $\approx 0.1$ , roughly representative of NO/NO<sub>2</sub> ratios in ambient conditions<sup>27</sup>), the only source of NO was from the photolysis of the RONO precursor, resulting in a steady-state concentration of  $\sim 40$  ppb with the lights on. (Full NO/NO<sub>2</sub> ratios throughout a typical experiment are provided in the Supporting Information.) At these classically high-NO conditions, reactions with HO<sub>2</sub> and isomerization reactions cannot compete with the RO<sub>2</sub> + NO pathway.<sup>28–30</sup> In addition to restricting accessible RO<sub>2</sub> reaction pathways, these high-NO concentrations further limit reaction complexity by shortening the lifetime of secondary oxidants O<sub>3</sub> and NO<sub>3</sub>, which could otherwise contribute to oxidation and SOA formation.<sup>31</sup> However, as described below, there is still sufficient secondary OH formation in the reaction mixture to affect the product distributions.

Prior to injection of RONO, the chamber was filled with dry ammonium sulfate seed particles to provide surface area to promote condensation of low-volatility products and to allow for correction for particle losses due to dilution and wall loss. Polydisperse (NH<sub>4</sub>)<sub>2</sub>SO<sub>4</sub> seed was added to the system by atomizing a 1 g L<sup>-1</sup> aqueous solution with a constant output atomizer (TSI) and passing the output through a desiccant prior to entering the chamber. Following this,  $\sim 400$  ppb of the RONO compound (described below) was injected into a septum and carried by a stream of air into the chamber where

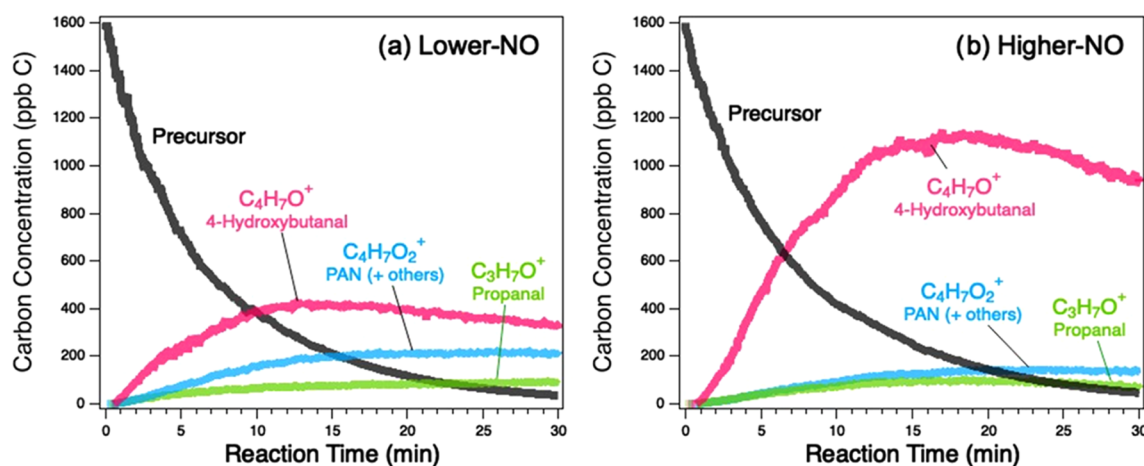


**Figure 2.** Carbon-weighted concentrations of the precursor and the three major product ions from the photolysis of *n*-butyl nitrite under (a) lower-NO and (b) higher-NO conditions, as measured by Vocus-PTR. Traces are labeled with the ion detected by the Vocus and the corresponding chemical identity; see the [Supporting Information](#) for a detailed discussion of molecular assignments for Vocus ions.

it was allowed to mix in the dark for 2 min. Finally, the lights were turned on to initiate the reaction and remained on for the duration of the experiment (approximately 1 h).

**Instrumentation.** Product distributions were measured by two real-time mass spectrometric instruments. Particle mass and composition were measured by an aerodyne high-resolution aerosol mass spectrometer (AMS),<sup>32</sup> run in a “V mode” (mass resolving power of  $\sim 3000$ ). The known ion fragmentation of various ions detected by the AMS enabled the extraction of the elemental ratios H/C and O/C,<sup>33</sup> thereby allowing the ensemble oxidation state of the SOA to be measured throughout the course of the reaction.<sup>34</sup> AMS organic signal was normalized to sulfate concentration to account for chamber dilution, wall loss, and changes in the AMS collection efficiency.

Products in the gas phase were measured by a Vocus proton-transfer reaction high-resolution time-of-flight mass spectrometer (PTR-MS),<sup>35</sup> which is capable of providing speciated measurements of individual molecules and is exceptionally sensitive to volatile compounds with relatively low carbon oxidation states.<sup>36</sup> To maximize its sensitivity to low-volatility compounds, the Vocus inlet is heated to 100 °C to reduce wall losses due to gas–wall partitioning. (The loss of gas-phase species to chamber walls and instrument inlets is expected to be minor in these experiments, as described in the [Supporting Information](#).) The pure RONO precursor is itself only weakly detected by the Vocus as a protonated molecule ( $[M + H]^+$ ); it is instead primarily detected as a combination of an aldehyde (via loss of  $-\text{NO}$ ,  $[M - \text{NO}]^+$ ) and an alkene (via loss of  $-\text{ONO}$ ,  $[M - \text{ONO}]^+$ ), as observed in previous work.<sup>37</sup> One challenge is that the aldehyde species is also a product formed from the oxidation of the alkoxy radical. To deconvolute the contributions to this ion from the RONO precursor and aldehyde product, the aldehyde time series was fit with a function that included a decay factor for the precursor and a growth factor for the product, as shown in [Figure S4](#).

The Vocus was calibrated by equating the total precursor signal (counts per second) prior to photolysis to the known amount of precursor injected into the chamber ( $\sim 400$  ppb); this ratio was then directly applied to all product compounds as an approximate calibration factor. Given the relatively limited range of oxidized functionalities and the tendency of PTR calibration factors to vary only up to a factor of  $\sim 2$  in

either direction,<sup>38</sup> the use of a single calibration factor for all species is assumed to be a reasonable approximation. While this approach introduces some error into the quantification of individual product species, differences in measured levels of a given compound in both the higher- and lower-NO experiments are independent of calibration, thus allowing for a direct comparison between experiments run under different NO/NO<sub>2</sub> ratios.

In addition to the mass spectrometric measurements of the organic species, concentrations of NO and NO<sub>2</sub> were measured with one of two NO<sub>x</sub> monitors (Thermo Fisher Scientific, Model 42i for measuring NO and NO<sub>x</sub>, or 2B Technologies Model 405 nm for measuring NO and NO<sub>2</sub>; see the [Supporting Information](#) for more details). The presence of NO<sub>y</sub> in the chamber interfered with precise NO<sub>2</sub> measurements (details regarding the deconvolution of interfering RONO signal from the pure NO<sub>x</sub> signal can be found in the [Supporting Information](#)); however, an order-of-magnitude difference in NO/NO<sub>2</sub> ratios between the two sets of experiments was still clearly observed. All gas-phase data collected by the NO<sub>x</sub> monitor and Vocus-PTR were corrected for dilution (with the exception of NO in the higher-NO experiments, in which it is part of the dilution flow) using an experiment-specific dilution rate based on chamber volume and input flow rates.

**Alkyl Nitrite Precursors.** Experiments were carried out with four straight-chain alkyl nitrites (*n*-butyl, *n*-pentyl, *n*-hexyl, and *n*-decyl nitrites). This study focuses on *n*-butyl nitrite as a simple model for gas-phase systems; *n*-pentyl nitrite was employed to examine trends across another gas-phase system, whereas the larger nitrites (*n*-hexyl and *n*-decyl nitrites) were studied to examine SOA formation.<sup>23,39,40</sup>

*N*-butyl nitrite and *n*-pentyl nitrite were purchased directly (Sigma-Aldrich) and used without further purification; *n*-hexyl nitrite and *n*-decyl nitrite were not commercially available and so were synthesized in the laboratory. Synthesis of alkyl nitrites was carried out by O-nitrosation of the parent alcohol species (Sigma-Aldrich), as described elsewhere.<sup>23,41,42</sup> Confirmation of the conversion of alcohol to alkyl nitrite was made by UV–vis spectroscopy of the RONO mixture, with spectra similar to those reported by Hecklen.<sup>26</sup> After synthesis, RONO species were wrapped in foil to limit exposure to ambient light and stored in the refrigerator until they were used in an experiment,

which typically occurred within 3 h of synthesis to maintain integrity.

**Master Chemical Mechanism Simulations.** Simulations using the Master Chemical Mechanism (MCM v3.2)<sup>43,44</sup> run using the FOAM package<sup>45</sup> in MATLAB were employed to map out the reaction mechanisms for individual NO regimes and precursors. These simulations were exploited to further probe differences between lower- and higher-NO conditions and for estimating species that are not detectable by our instruments (e.g., OH).

Because the precursor RONO species used in these experiments are not included in the MCM, the experimentally determined photolysis rate of the RONO (as measured by the Vocus) was used to introduce RO and NO into the simulation at a controlled rate; in higher-NO experiments, the concentration of NO in the simulation was fixed at 1 ppm. Simulations included a dilution factor to recreate chamber conditions.

## RESULTS AND DISCUSSION

Average NO/NO<sub>2</sub> ratios are determined by comparisons of NO<sub>x</sub> monitor measurements and MCM simulations. For lower-NO experiments, the NO/NO<sub>2</sub> ratio quickly reaches a steady-state value of ~0.1 with the lights turned on; for higher-NO experiments, a constant flow of 1 ppm NO into the chamber results in NO/NO<sub>2</sub> > 1 throughout the experiment (Table S1 and Figures S1 and S2).

Figure 2 shows the major gas-phase products (weighted by ppb carbon) from the photolysis of *n*-butyl nitrite under lower-NO (panel a) and higher-NO (panel b) conditions. These major ions account for ~60% (lower-NO) and ~75% (higher-NO) of measured secondary carbon; stacked plots of all detected product traces are provided in Figure S5. In both experiments, the precursor reacts away at a roughly equivalent rate (average decay constant of  $\sim 2 \times 10^{-3} \text{ s}^{-1}$ ), which is also the case for all other precursors in these experiments; this decay is consistent with precursor loss by photolysis that exhibits no dependence on NO. While the precursor RONO is capable of reacting directly with OH generated in the reaction mixture, the concentrations of OH (predicted by MCM simulations and shown in Figure S6) and small rate constant ( $k_{\text{RONO}+\text{OH}} < 3 \times 10^{-12} \text{ cm}^3 \text{ mol}^{-1} \text{ s}^{-1}$ )<sup>46</sup> suggest that this pathway is minor, accounting for only 5–10% of RONO loss.

The RO radicals formed from RONO photolysis are expected to undergo the same reactions in both the lower-NO and higher-NO experiments (Figure 1). A fraction (~20%) of the RO radicals are expected to react directly with O<sub>2</sub> to form butanal, but because the detected ion is the same as one of the ions from the precursor (as discussed above), the exact contribution of this minor channel is not well constrained in these experiments. The majority of the RO radicals will isomerize, forming a hydroxy-substituted RO<sub>2</sub> radical. The high concentration of NO in both cases ensures that this RO<sub>2</sub> will react with NO, predominantly forming 4-hydroxybutanal (C<sub>4</sub>H<sub>8</sub>O<sub>2</sub>, primarily detected as the dehydrated C<sub>4</sub>H<sub>7</sub>O<sup>+</sup> ion by the Vocus<sup>47</sup>). A fraction of the RO<sub>2</sub> will react with NO to form the 4-hydroxynitrate product (C<sub>4</sub>H<sub>9</sub>NO<sub>4</sub>), but the yield is expected to be very small (~1%),<sup>5</sup> and such oxygenated nitrates are poorly detected by the Vocus.<sup>36</sup> The other RO<sub>2</sub> channels are not expected to be competitive: under both lower- and higher-NO conditions, the RO<sub>2</sub> + HO<sub>2</sub>, RO<sub>2</sub> + RO<sub>2</sub>, and RO<sub>2</sub> isomerization channels are expected to contribute negligibly (<<1%) to the reaction, and the

peroxynitrate formed from RO<sub>2</sub> + NO<sub>2</sub> is too short-lived to contribute to the reaction mixture.<sup>5,20</sup>

Despite the identical chemistry of the initially formed RO and RO<sub>2</sub> radicals under the two NO regimes, there are substantial differences in their product distributions (Figure 2). (These differences are much larger than expected run-to-run variability, as duplicate runs show very little variation, as shown in Figure S7.) Most notably, while the major product in both cases is 4-hydroxybutanal (C<sub>4</sub>H<sub>7</sub>O<sup>+</sup>), it is present in much greater concentrations under higher-NO conditions. This disparity arises from differences not in formation yield but in loss rates; as shown in Figure S8, the initial formation rate of this compound is the same in the two cases, as expected from the RO<sub>2</sub> chemistry (Figure 1). Because the main chemical sink of hydroxybutanal is oxidation by OH (photolysis is only a very minor channel, estimated to be ~2% by MCM), the more rapid loss of this species under lower-NO conditions implies that lower-NO experiments involve higher concentrations of OH.

While the reaction system used here did not involve the initial generation of OH, secondary OH can be formed from the reaction of HO<sub>2</sub> (formed after the isomerization of the hydroxyalkoxy radical; Figure 1) with NO. MCM simulations predict that, under higher-NO conditions, OH is produced at a greater rate (by a factor of ~2.5) but that the OH reactivity is higher still (largely due to increased NO<sub>x</sub> levels), leading to lower levels of OH overall (Figure S6). The prediction of higher OH levels under lower-NO conditions is further confirmed by the higher mean carbon oxidation state ( $\overline{\text{OS}}_{\text{C}}$ )<sup>34</sup> of the measured product distribution under lower-NO conditions; this trend of increased oxidation under lower-NO/NO<sub>2</sub> ratios is also observed for the photolysis of *n*-pentyl nitrite (Figure S9).

The photolysis of *n*-butyl nitrite produces no observable SOA, consistent with the small carbon skeleton and consequently high volatility of the products formed. Larger nitrites (*n*<sub>C</sub> > 5), however, can form products with sufficiently low volatilities to contribute to the formation of SOA.<sup>23,40</sup> This is evident from Figure 3, which shows SOA formation from the photolysis of *n*-pentyl nitrite, *n*-hexyl nitrite, and *n*-decyl nitrite under lower- and higher-NO conditions. As in the gas phase, the particle-phase measurements exhibit differences under the two NO regimes. All three precursors exhibit higher SOA production under lower-NO conditions as measured in the plateau region (i.e., after 10 min). Most notably, *n*-pentyl nitrite produces no measurable SOA under higher-NO conditions but measurable levels under lower-NO conditions. Additionally, *n*-hexyl nitrite and *n*-decyl nitrite produce approximately 64 and 78% more SOA under lower-NO conditions, respectively. (As shown in the Supporting Information, the observed differences are greater than the uncertainty in the measurements.) As with results in the gas phase, this can be attributed to higher levels of secondary OH under lower-NO conditions, leading to more highly oxidized products that partition into the particle phase. This observation is also in agreement with previous studies that see SOA yields for most systems as being inversely correlated with NO concentrations.<sup>12,19</sup> Further, the mean oxidation state of measured SOA formed from *n*-decyl nitrite (the only precursor for which SOA formation is large enough for a precise measurement of  $\overline{\text{OS}}_{\text{C}}$ ) is greater under lower-NO conditions (−1.34) than under higher-NO conditions

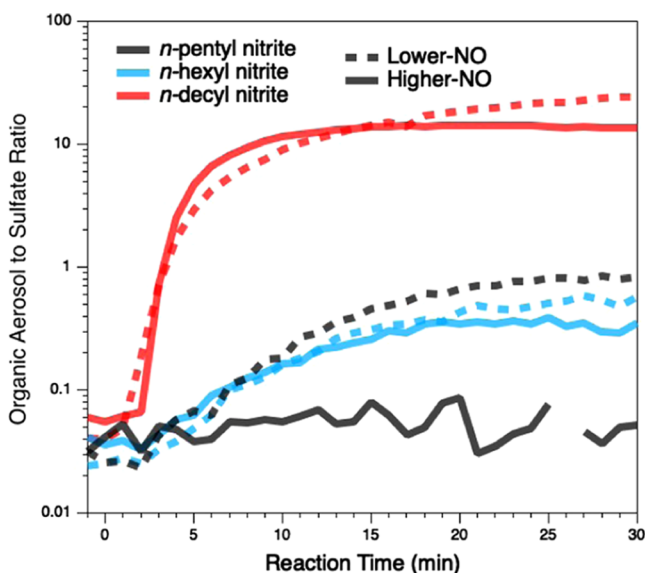


**Figure 3.** AMS total organic time series under lower-NO (dashed lines) and higher-NO (solid lines) concentrations. Traces are normalized to sulfate concentration to account for wall losses, collection efficiency, and dilution. *N*-butyl nitrite produces no organic aerosol, similar to *n*-pentyl nitrite under higher-NO conditions, and so it is not shown.

(−1.45); this is consistent with the observed mean oxidation states in the gas-phase product distributions.

The difference in OH in the lower-NO and higher-NO experiments thus leads to differences in the formation of later-generation products, the extent of oxidation of the product distribution, and the formation of SOA. While this effect is mostly important in laboratory studies (this chemistry does not have a controlling influence on OH in the atmosphere), the NO/NO<sub>2</sub> ratio is likely to affect product distributions via other effects as well. To further investigate the influence of NO<sub>x</sub> on VOC oxidation product distributions, Figure 4a compares the

average (carbon-weighted) concentrations of different gas-phase products from *n*-butyl nitrite photolysis under the two different NO/NO<sub>2</sub> ratios. The higher-NO regime is characterized by a dominant concentration of 4-hydroxybutanal (C<sub>4</sub>H<sub>7</sub>O<sup>+</sup>) due to lower levels of OH and therefore a longer lifetime, as discussed above (Figures 2 and S8). Conversely, greater OH concentrations under lower-NO conditions result in a wider variety of products and greater concentrations of products with higher oxidation states (Figures 4 and S10), providing the basis for the larger  $\overline{OS}_C$  (Figure S9). This includes multigenerational oxidation products such as propanal (C<sub>3</sub>H<sub>7</sub>O<sup>+</sup>, formed from the reaction of butanal + OH), which has a greater concentration under lower-NO conditions (Figures 2 and 4).

Figure 4b shows the same comparison of product distributions in the two NO regimes but based on MCM predictions rather than experimental data. While detailed comparisons between Vocus and MCM distributions are beyond the scope of this work, the fact that the MCM predicts fewer major products than are measured by the Vocus is likely attributable to individual molecules being detected as multiple fragment ions by the Vocus and to the generally simplified chemistry of the MCM. Overall consistencies between the MCM simulations and Vocus data include a predominance of 4-hydroxybutanal (C<sub>4</sub>H<sub>8</sub>O<sub>2</sub>) occurring under both NO regimes, with a greater concentration of this species under higher-NO conditions. These general results are similar to those from the *n*-pentyl nitrite system (Figures S11 and S12).

The most pronounced differences between the two NO<sub>x</sub> regimes in Figure 4b are the PAN compounds (e.g., C<sub>4</sub>H<sub>7</sub>NO<sub>6</sub>), which are considerably more prevalent under lower-NO conditions and, as discussed below, are second-generation oxidation products. PANs are not detected directly by PTR-MS but can be detected by known fragmentation patterns.<sup>48–50</sup> One example is C<sub>4</sub>H<sub>7</sub>O<sub>2</sub><sup>+</sup>, a predicted tracer ion for C<sub>4</sub>H<sub>7</sub>NO<sub>6</sub> (analogous to C<sub>2</sub>H<sub>3</sub>O<sup>+</sup> serving as a tracer ion for peroxyacetyl nitrate, C<sub>2</sub>H<sub>3</sub>NO<sub>5</sub>);<sup>48</sup> its identity as a PAN is further suggested by the induction period observed in its time

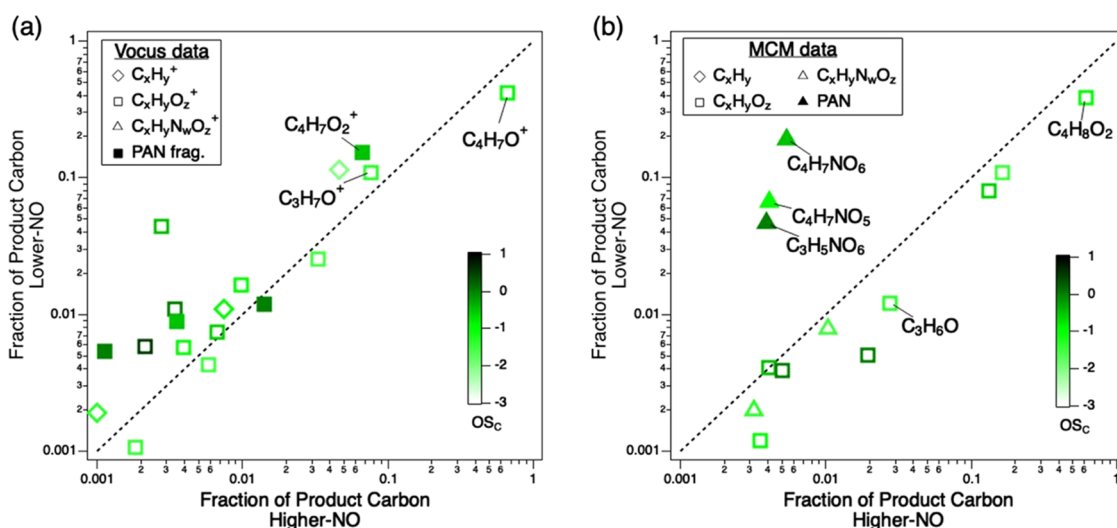
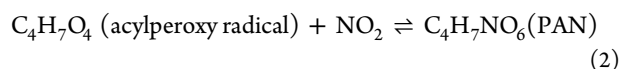
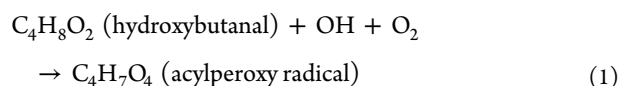


**Figure 4.** Correlation plots for fractions of gas-phase products under lower-NO vs higher-NO regimes, averaged over the entire experiment. Panel (a) Vocus-PTR observations. Panel (b) MCM predictions. Markers are shaped according to the class of molecule and are colored by the mean carbon oxidation state ( $\overline{OS}_C$ ). Labeled compounds in panel (a) are the same as those in Figure 2; all other compounds are discussed in detail in the Supporting Information. MCM results (panel b) include labels for peroxyacetyl nitrate (PAN) species (solid triangles); potential PAN fragments are represented by filled markers in panel (a). The dashed line represents the 1:1 ratio.

series (Figure 2), which is indicative of later-generation products. Potential PAN fragments are represented by shaded squares in Figure 4a. (A more detailed discussion of these other PAN-related ions detected by the Vocus can be found in the Supporting Information.) Although these compounds are more prevalent under lower-NO conditions, the measured differences are not as dramatic as predicted by MCM simulations. This may be because these ions are not unique to PAN fragments, as they may be formed from the fragmentation of other product ions (e.g., acyl compounds), potentially resulting in a shift toward the 1:1 line. For example, while  $C_4H_7O_2^+$  is a tracer for  $C_4H_7NO_6$ , it could be a tracer for 4-hydroxybutanoic acid and similar species as well.

PAN formation, from the reaction of acylperoxy radicals with  $NO_2$ , is not shown in Figure 1, since acylperoxy radicals are not formed as first-generation radicals from alkoxy radical isomerization. Instead, acylperoxy radicals will be formed from the oxidation of first-generation aldehyde species, such as 4-hydroxybutanal:



Rates of PAN formation are observed (Figure 4a) and predicted (Figure 4b) to be substantially greater under lower-NO conditions. This is a result of two factors: the difference in OH levels (as discussed above), which controls the formation of acylperoxy radicals, and the subsequent chemistry of the acylperoxy radical. When  $NO_x$  is present, acylperoxy radicals are limited to two reactions: reaction with  $NO_2$  to form PAN and reaction with NO to form acyloxy radicals. The concentrations of PAN species are thus a strong function of the  $NO/NO_2$  ratio, as discussed elsewhere.<sup>4,14,19,20</sup> Under higher-NO conditions, this ratio is sufficiently high ( $NO/NO_2 > 1$ ) that the acylperoxy + NO pathway is dominant, limiting the formation of PAN. Under lower-NO conditions ( $NO/NO_2 \approx 0.1$ ), there is considerable competition from the acylperoxy +  $NO_2$  pathway, resulting in the accumulation of PAN species. Thus, PAN formation is more favored under lower-NO than under higher-NO conditions because it fosters higher OH levels and a greater rate of the acylperoxy +  $NO_2$  reaction. This additional PAN formation, which is observed in the measurements and predicted by MCM simulations (Figure 4), sequesters  $RO_2$  radicals from the reaction mixture, terminating the oxidation chain and decreasing the extent to which subsequent chemistry occurs over the time scales of the experiments.<sup>4,14,20</sup>

## ■ IMPLICATIONS

These results are broadly consistent with previous studies that demonstrate the importance of  $NO_x$  in controlling product distributions, beyond the prevailing  $RO_2 + NO$  reaction in high-NO systems. Hoffmann et al.<sup>21</sup> suggested the role of  $NO_x$  in controlling the relative concentrations of secondary oxidants and the subsequent influence on SOA formation. A number of recent studies have examined the specific role that PAN formation and the  $NO/NO_2$  ratio may play in laboratory studies of hydrocarbon oxidation. Chan et al.<sup>19</sup> demonstrated the importance of the  $NO/NO_2$  ratio in governing SOA production from isoprene oxidation, in which PAN is an

intermediate in SOA formation. Specifically, they found that even under high-NO conditions, low  $NO/NO_2$  ratios foster increased production of PAN, which subsequently contributes to SOA generation. Rissanen et al.<sup>20</sup> expanded on that work by characterizing the individual contributions of NO and  $NO_2$  in the formation of highly oxidized multifunctional compounds (HOMs), finding that the  $NO/NO_2$  ratio effectively controls the identities of HOMs in oxidation systems. Similarly, the modeling study of Peng et al.<sup>4</sup> highlighted the importance of accurately representing  $NO_x$  chemistry (including PAN formation) and oxidant levels in oxidation flow reactors (typically used for measurements of SOA formation) to reflect atmospheric conditions.

This work builds on these previous studies by showing that the entire product distribution (not only the formation of HOMs and SOA) can be impacted by  $NO_x$  effects that go beyond the standard  $RO_2$  branching ( $RO_2 + NO$  vs.  $RO_2 + HO_2$  vs.  $RO_2$  isomerization). We find that, even in a high-NO regime, a lower- $NO/NO_2$  ratio fosters higher concentrations of secondary OH, higher PAN concentrations, and a more highly oxidized product distribution. Together, these results can affect the entire product distribution in chamber experiments, leading to a potential disconnect between chamber results and product distributions expected in the atmosphere.

PAN plays an important role in atmospheric systems by sequestering  $HO_x$  and  $NO_x$ , thereby influencing the kinetics of organic carbon evolution. Here, PAN formation is observed to be highly sensitive to the  $NO/NO_2$  ratio. Under lower-NO conditions, PAN is observed to form preferentially, limiting the extent of subsequent chemistry. As such, PAN formation can affect SOA formation even when it does not serve as a direct intermediate in SOA formation (as is the case in isoprene oxidation<sup>19</sup>). This has implications for recreating high-NO atmospheric conditions in chamber experiments. Specifically, when trying to achieve polluted conditions, it is not sufficient to flood the reactor with NO; while this ensures that  $RO_2 + HO_2$  and  $RO_2$  isomerization reactions cannot compete with  $RO_2 + NO$ , it risks leading to PAN concentrations that may not be representative of atmospheric conditions. Rather, the atmospheric  $NO/NO_2$  ratio has an important influence on the relevance of chamber results to atmospheric conditions; a lower- $NO/NO_2$  ratio results in increased levels of SOA (via the increasingly competitive  $RO_2 + NO_2$  reaction channel), while a higher- $NO/NO_2$  ratio results in fewer products and lower mean oxidation states. This work therefore highlights the need for experimental studies of product distributions and SOA formation to be carried out under atmospherically relevant  $NO/NO_2$  ratios. This has been suggested previously for the accurate simulation of SOA and HOM formation;<sup>19,20</sup> here, we show that the use of atmospherically relevant  $NO/NO_2$  ratios is important in virtually all oxidation systems to better simulate the complex, multiphase product distributions generated during atmospheric oxidation processes. It is thus important that laboratory product studies be carried out under conditions in which both the  $NO/NO_2$  ratio and  $RO_2$  chemistry are accurately representative of the atmosphere. Both the absolute  $NO_x$  level and the  $NO/NO_2$  ratios may be important in controlling product distributions, and future study of these effects should focus on how product distributions depend on both.

## ■ ASSOCIATED CONTENT

### Supporting Information

The Supporting Information is available free of charge at <https://pubs.acs.org/doi/10.1021/acs.est.0c07621>.

Molecular assignments of PTR data; concentrations of NO and NO<sub>2</sub> for each of the experiments (Table S1; Figures S1 and S2); discussion of wall and tubing losses (Figure S3); deconvolution of precursor and product contributions to C<sub>4</sub>H<sub>7</sub>O<sup>+</sup> (Figure S4); PTR stacked plots for *n*-butyl nitrite photolysis (Figure S5); concentrations, sources, and sinks of OH in *n*-butyl nitrite photolysis as predicted by MCM simulations (Figure S6); experimental uncertainty and reproducibility (Figure S7); C<sub>4</sub>H<sub>7</sub>O<sup>+</sup> product time series under different NO/NO<sub>2</sub> ratios (Figure S8); oxidation states of gas-phase product distributions (Figure S9); detailed correlation plots for the photolysis of *n*-butyl nitrite (Figure S10); and product distributions from the photolysis *n*-pentyl nitrite (Figures S11 and S12) (PDF)

## ■ AUTHOR INFORMATION

### Corresponding Author

Kevin J. Nihill – Department of Civil and Environmental Engineering, Massachusetts Institute of Technology, Cambridge, Massachusetts 02139, United States; Email: [kevin.j.nihill@gmail.com](mailto:kevin.j.nihill@gmail.com)

### Authors

Qing Ye – Department of Civil and Environmental Engineering, Massachusetts Institute of Technology, Cambridge, Massachusetts 02139, United States

Francesca Majluf – Aerodyne Research, Inc., Billerica, Massachusetts 01821, United States; [orcid.org/0000-0002-7688-1452](https://orcid.org/0000-0002-7688-1452)

Jordan E. Krechmer – Aerodyne Research, Inc., Billerica, Massachusetts 01821, United States; [orcid.org/0000-0003-3642-0659](https://orcid.org/0000-0003-3642-0659)

Manjula R. Canagaratna – Aerodyne Research, Inc., Billerica, Massachusetts 01821, United States

Jesse H. Kroll – Department of Civil and Environmental Engineering, Massachusetts Institute of Technology, Cambridge, Massachusetts 02139, United States; [orcid.org/0000-0002-6275-521X](https://orcid.org/0000-0002-6275-521X)

Complete contact information is available at: <https://pubs.acs.org/doi/10.1021/acs.est.0c07621>

### Notes

The authors declare no competing financial interest.

## ■ ACKNOWLEDGMENTS

This work was supported by NSF grant CHE-1709993. The authors also wish to acknowledge Josh Moss for his insight into MCM simulations and PTR fragmentation patterns, Andrew Lambe and Anthony Carrasquillo for their assistance in precursor synthesis, and Megan Claflin for sharing her knowledge on detection of alkyl nitrites in the PTR.

## ■ REFERENCES

(1) Lannuque, V.; Camredon, M.; Couvidat, F.; Hodzic, A.; Valorso, R.; Madronich, S.; Bessagnet, B.; Aumont, B. Exploration of the Influence of Environmental Conditions on Secondary Organic

Aerosol Formation and Organic Species Properties Using Explicit Simulations: Development of the VBS-GECKO Parameterization. *Atmos. Chem. Phys.* **2018**, *18*, 13411–13428.

(2) Goldstein, A. H.; Galbally, I. E. Known and Unexplored Organic Constituents in the Earth's Atmosphere. *Environ. Sci. Technol.* **2007**, *41*, 1514–1521.

(3) Hallquist, M.; Wenger, J. C.; Baltensperger, U.; Rudich, Y.; Simpson, D.; Claeys, M.; Dommen, J.; Donahue, N. M.; George, C.; Goldstein, A. H.; Hamilton, J. H.; Herrmann, H.; Hoffmann, T.; Iinuma, Y.; Jang, M.; Jenkin, M. E.; Jimenez, J. L.; Kiendler-Scharr, A.; Maenhaut, W.; McFiggans, G.; Mentel, ThF.; Monod, A.; Prévôt, A. S. H.; Seinfeld, J. H.; Surratt, J. D.; Szmigielski, R.; Wildt, J. The Formation, Properties and Impact of Secondary Organic Aerosol: Current and Emerging Issues. *Atmos. Chem. Phys.* **2009**, *9*, 5155–5236.

(4) Peng, Z.; Lee-Taylor, J.; Orlando, J. J.; Tyndall, G. S.; Jimenez, J. L. Organic Peroxy Radical Chemistry in Oxidation Flow Reactors and Environmental Chambers and Their Atmospheric Relevance. *Atmos. Chem. Phys.* **2019**, *19*, 813–834.

(5) Orlando, J. J.; Tyndall, G. S. Laboratory Studies of Organic Peroxy Radical Chemistry: An Overview with Emphasis on Recent Issues of Atmospheric Significance. *Chem. Soc. Rev.* **2012**, *41*, 6294–6317.

(6) Crouse, J. D.; Nielsen, L. B.; Jørgensen, S.; Kjaergaard, H. G.; Wennberg, P. O. Autoxidation of Organic Compounds in the Atmosphere. *J. Phys. Chem. Lett.* **2013**, *4*, 3513–3520.

(7) Lelieveld, J.; Butler, T. M.; Crowley, J. N.; Dillon, T. J.; Fischer, H.; Ganzeveld, L.; Harder, H.; Lawrence, M. G.; Martinez, M.; Taraborrelli, D.; Williams, J. Atmospheric Oxidation Capacity Sustained by a Tropical Forest. *Nature* **2008**, *452*, 737–740.

(8) Ren, X.; Harder, H.; Martinez, M.; Leshner, R. L.; Olinger, A.; Shirley, T.; Adams, J.; Simpasa, J. B.; Brune, W. H. HO<sub>x</sub> Concentrations and OH Reactivity Observations in New York City during PMTACS-NY2001. *Atmos. Environ.* **2003**, *37*, 3627–3637.

(9) Martinsson, J.; Eriksson, A. C.; Nielsen, I. E.; Malmberg, V. B.; Ahlberg, E.; Andersen, C.; Lindgren, R.; Nyström, R.; Nordin, E. Z.; Brune, W. H.; Svenningsson, B.; Swietlicki, E.; Boman, C.; Pagels, J. H. Impacts of Combustion Conditions and Photochemical Processing on the Light Absorption of Biomass Combustion Aerosol. *Environ. Sci. Technol.* **2015**, *49*, 14663–14671.

(10) Tkacik, D. S.; Lambe, A. T.; Jathar, S.; Li, X.; Presto, A. A.; Zhao, Y.; Blake, D. R.; Meinardi, S.; Jayne, J. T.; Croteau, P. L.; Robinson, A. L. Secondary Organic Aerosol Formation from In-Use Motor Vehicle Emissions Using a Potential Aerosol Mass Reactor. *Environ. Sci. Technol.* **2014**, *48*, 11235–11242.

(11) Ortega, A. M.; Day, D. A.; Cubison, M. J.; Brune, W. H.; Bon, D.; De Gouw, J. A.; Jimenez, J. L. Secondary Organic Aerosol Formation and Primary Organic Aerosol Oxidation from Biomass-Burning Smoke in a Flow Reactor during FLAME-3. *Atmos. Chem. Phys.* **2013**, *13*, 11551–11571.

(12) Kroll, J. H.; Ng, N. L.; Murphy, S. M.; Flagan, R. C.; Seinfeld, J. H. Secondary Organic Aerosol Formation from Isoprene Photooxidation. *Environ. Sci. Technol.* **2006**, *40*, 1869–1877.

(13) Crouse, J. D.; Paulot, F.; Kjaergaard, H. G.; Wennberg, P. O. Peroxy Radical Isomerization in the Oxidation of Isoprene. *Phys. Chem. Chem. Phys.* **2011**, *13*, 13607–13613.

(14) Peng, Z.; Jimenez, J. L. Modeling of the Chemistry in Oxidation Flow Reactors with High Initial NO. *Atmos. Chem. Phys.* **2017**, *17*, 11991–12010.

(15) Kroll, J. H.; Seinfeld, J. H. Chemistry of Secondary Organic Aerosol: Formation and Evolution of Low-Volatility Organics in the Atmosphere. *Atmos. Environ.* **2008**, *42*, 3593–3624.

(16) Ziemann, P. J.; Atkinson, R. Kinetics, Products, and Mechanisms of Secondary Organic Aerosol Formation. *Chem. Soc. Rev.* **2012**, *41*, 6582–6605.

(17) Arey, J.; Aschmann, S. M.; Kwok, E. S. C.; Atkinson, R. Alkyl Nitrate, Hydroxyalkyl Nitrate, and Hydroxycarbonyl Formation from the NO<sub>x</sub>-Air Photooxidations of C<sub>5</sub>–C<sub>8</sub> *n*-Alkanes. *J. Phys. Chem. A* **2001**, *105*, 1020–1027.

- (18) Zhang, X.; Cappa, C. D.; Jathar, S. H.; McVay, R. C.; Ensberg, J. J.; Kleeman, M. J.; Seinfeld, J. H. Influence of Vapor Wall Loss in Laboratory Chambers on Yields of Secondary Organic Aerosol. *Proc. Natl. Acad. Sci. U.S.A.* **2014**, *111*, 5802–5807.
- (19) Chan, A. W. H.; Chan, M. N.; Surratt, J. D.; Chhabra, P. S.; Loza, C. L.; Crounse, J. D.; Yee, L. D.; Flagan, R. C.; Wennberg, P. O.; Seinfeld, J. H. Role of Aldehyde Chemistry and NO<sub>x</sub> Concentrations in Secondary Organic Aerosol Formation. *Atmos. Chem. Phys.* **2010**, *10*, 7169–7188.
- (20) Rissanen, M. P. NO<sub>2</sub> Suppression of Autoxidation – Inhibition of Gas-Phase Highly Oxidized Dimer Product Formation. *ACS Earth Space Chem.* **2018**, *2*, 1211–1219.
- (21) Hoffmann, T.; Odum, J. A. Y. R.; Bowman, F.; Collins, D.; Klockow, D.; Flagan, R. C.; Seinfeld, J. H. Formation of Organic Aerosols from the Oxidation of Biogenic Hydrocarbons. *J. Atmos. Chem.* **1997**, *26*, 189–222.
- (22) Kessler, S. H.; Nah, T.; Carrasquillo, A. J.; Jayne, J. T.; Worsnop, D. R.; Wilson, K. R.; Kroll, J. H. Formation of Secondary Organic Aerosol from the Direct Photolytic Generation of Organic Radicals. *J. Phys. Chem. Lett.* **2011**, *2*, 1295–1300.
- (23) Carrasquillo, A. J.; Hunter, J. F.; Daumit, K. E.; Kroll, J. H. Secondary Organic Aerosol Formation via the Isolation of Individual Reactive Intermediates: Role of Alkoxy Radical Structure. *J. Phys. Chem. A* **2014**, *118*, 8807–8816.
- (24) Carrasquillo, A. J.; Daumit, K. E.; Kroll, J. H. Radical Reactivity in the Condensed Phase: Intermolecular versus Intramolecular Reactions of Alkoxy Radicals. *J. Phys. Chem. Lett.* **2015**, *6*, 2388–2392.
- (25) Lim, C. Y.; Hagan, D. H.; Coggon, M. M.; Koss, A. R.; Sekimoto, K.; De Gouw, J. A.; Warneke, C.; Cappa, C. D.; Kroll, J. H. Secondary Organic Aerosol Formation from the Laboratory Oxidation of Biomass Burning Emissions. *Atmos. Chem. Phys.* **2019**, *19*, 12797–12809.
- (26) Hecklen, J. The Decomposition of Alkyl Nitrites and the Reaction of Alkoxy Radicals. *Adv. Photochem.* **1988**, *14*, 177–272.
- (27) Silvern, R. F.; Jacob, D. J.; Travis, K. R.; Sherwen, T.; Evans, M. J.; Cohen, R. C.; Laughner, J. L.; Hall, S. R.; Ullmann, K.; Crounse, J. D.; Wennberg, P. O.; Peischl, J.; Pollack, I. B. Observed NO/NO<sub>2</sub> Ratios in the Upper Troposphere Imply Errors in NO-NO<sub>2</sub>-O<sub>3</sub> Cycling Kinetics or an Unaccounted NO<sub>x</sub> Reservoir. *Geophys. Res. Lett.* **2018**, *45*, 4466–4474.
- (28) Denisova, T. G.; Denisov, E. T. Kinetic Parameters of Alkyl, Alkoxy, and Peroxy Radical Isomerization. *Kinet. Catal.* **2001**, *42*, 620–630.
- (29) Praske, E.; Otkjær, R. V.; Crounse, J. D.; Hethcox, J. C.; Stoltz, B. M.; Kjaergaard, H. G.; Wennberg, P. O. Atmospheric Autoxidation Is Increasingly Important in Urban and Suburban North America. *Proc. Natl. Acad. Sci. U.S.A.* **2018**, *115*, 64–69.
- (30) Otkjær, R. V.; Jakobsen, H. H.; Tram, C. M.; Kjaergaard, H. G. Calculated Hydrogen Shift Rate Constants in Substituted Alkyl Peroxy Radicals. *J. Phys. Chem. A* **2018**, *122*, 8665–8673.
- (31) Griffin, R. J.; Cocker, D. R.; Flagan, R. C.; Seinfeld, J. H. Organic Aerosol Formation from the Oxidation of Biogenic Hydrocarbons. *J. Geophys. Res.* **1999**, *104*, 3555–3567.
- (32) DeCarlo, P. F.; Kimmel, J. R.; Trimborn, A.; Northway, M. J.; Jayne, J. T.; Aiken, A. C.; Gonin, M.; Fuhrer, K.; Horvath, T.; Docherty, K. S.; Worsnop, D. R.; Jimenez, J. L. Field-Deployable, High-Resolution, Time-of-Flight Aerosol Mass Spectrometer. *Anal. Chem.* **2006**, *78*, 8281–8289.
- (33) Canagaratna, M. R.; Jimenez, J. L.; Kroll, J. H.; Chen, Q.; Kessler, S. H.; Massoli, P.; Hildebrandt Ruiz, L.; Fortner, E.; Williams, L. R.; Wilson, K. R.; Surratt, J. D.; Donahue, N. M.; Jayne, J. T.; Worsnop, D. R. Elemental Ratio Measurements of Organic Compounds Using Aerosol Mass Spectrometry: Characterization, Improved Calibration, and Implications. *Atmos. Chem. Phys.* **2015**, *15*, 253–272.
- (34) Kroll, J. H.; Donahue, N. M.; Jimenez, J. L.; Kessler, S. H.; Canagaratna, M. R.; Wilson, K. R.; Altieri, K. E.; Mazzoleni, L. R.; Wozniak, A. S.; Bluhm, H.; Mysak, E. R.; Smith, J. D.; Kolb, C. E.; Worsnop, D. R. Carbon Oxidation State as a Metric for Describing the Chemistry of Atmospheric Organic Aerosol. *Nat. Chem.* **2011**, *3*, 133–139.
- (35) Krechmer, J. E.; Lopez-Hilfiker, F. D.; Koss, A. R.; Hutterli, M.; Stoermer, C.; Deming, B.; Kimmel, J. R.; Warneke, C.; Holzinger, R.; Jayne, J.; Worsnop, D.; Fuhrer, K.; Gonin, M.; de Gouw, J. Evaluation of a New Reagent-Ion Source and Focusing Ion–Molecule Reactor for Use in Proton-Transfer-Reaction Mass Spectrometry. *Anal. Chem.* **2018**, *90*, 12011–12018.
- (36) Isaacman-VanWertz, G.; Massoli, P.; O'Brien, R. E.; Nowak, J. B.; Canagaratna, M. R.; Jayne, J. T.; Worsnop, D. R.; Su, L.; Knopf, D. A.; Misztal, P.; Arata, C.; Goldstein, A. H.; Kroll, J. H. Using Advanced Mass Spectrometry Techniques to Fully Characterize Atmospheric Organic Carbon: Current Capabilities and Remaining Gaps. *Faraday Discuss.* **2017**, *200*, 579–598.
- (37) Aoki, N.; Inomata, S.; Tanimoto, H. Detection of C<sub>1</sub>–C<sub>5</sub> Alkyl Nitrates by Proton Transfer Reaction Time-of-Flight Mass Spectrometry. *Int. J. Mass Spectrom.* **2007**, *263*, 12–21.
- (38) Yuan, B.; Koss, A. R.; Warneke, C.; Coggon, M. M.; Sekimoto, K.; De Gouw, J. A. Proton-Transfer-Reaction Mass Spectrometry: Applications in Atmospheric Sciences. *Chem. Rev.* **2017**, *117*, 13187–13229.
- (39) Lim, Y. B.; Ziemann, P. J. Effects of Molecular Structure on Aerosol Yields from OH Radical-Initiated Reactions of Linear, Branched, and Cyclic Alkanes in the Presence of NO<sub>x</sub>. *Environ. Sci. Technol.* **2009**, *43*, 2328–2334.
- (40) Lim, Y. B.; Ziemann, P. J. Products and Mechanism of Secondary Organic Aerosol Formation from Reactions of *n*-Alkanes with OH Radicals in the Presence of NO<sub>x</sub>. *Environ. Sci. Technol.* **2005**, *39*, 9229–9236.
- (41) Hunter, J. F.; Carrasquillo, A. J.; Daumit, K. E.; Kroll, J. H. Secondary Organic Aerosol Formation from Acyclic, Monocyclic, and Polycyclic Alkanes. *Environ. Sci. Technol.* **2014**, *48*, 10227–10234.
- (42) Noyes, W. A. Explanation of the Formation of Alkyl Nitrites in Dilute Solutions; Butyl and Amyl Nitrites. *J. Am. Chem. Soc.* **1933**, *55*, 3888–3889.
- (43) Bloss, C.; Wagner, V.; Jenkin, M. E.; Volkamer, R.; Bloss, W. J.; Lee, J. D.; Heard, D. E.; Wirtz, K.; Rea, G.; Wenger, J. C.; Pilling, M. J.; Martin-Reviejo, M. Development of a Detailed Chemical Mechanism (MCMv3.1) for the Atmospheric Oxidation of Aromatic Hydrocarbons. *Atmos. Chem. Phys.* **2005**, *5*, 641–664.
- (44) Saunders, S. M.; Jenkin, M. E.; Derwent, R. G.; Pilling, M. J. Protocol for the Development of the Master Chemical Mechanism, MCM v3 (Part A): Tropospheric Degradation of Non-Aromatic Volatile Organic Compounds. *Atmos. Chem. Phys.* **2003**, *3*, 161–180.
- (45) Wolfe, G. M.; Marvin, M. R.; Roberts, S. J.; Travis, K. R.; Liao, J. The Framework for 0-D Atmospheric Modeling (FOAM) v3.1. *Geosci. Model Dev.* **2016**, *9*, 3309–3319.
- (46) Calvert, J. G.; Orlando, J. J.; Stockwell, W. R.; Wallington, T. J. *The Mechanisms of Reactions Influencing Atmospheric Ozone*; Oxford University Press, 2015.
- (47) Demarcke, M.; Amelynck, C.; Schoon, N.; Dhooghe, F.; Rimetz-Planchon, J.; Van Langenhove, H.; Dewulf, J. Laboratory Studies in Support of the Detection of Biogenic Unsaturated Alcohols by Proton Transfer Reaction-Mass Spectrometry. *Int. J. Mass Spectrom.* **2010**, *290*, 14–21.
- (48) Hastie, D. R.; Gray, J.; Langford, V. S.; Maclagan, R. G. A. R.; Milligan, D. B.; Mcewan, M. J. Real-Time Measurement of Peroxyacetyl Nitrate Using Selected Ion Flow Tube Mass Spectrometry. *Rapid Commun. Mass Spectrom.* **2010**, *24*, 343–348.
- (49) Hansel, A.; Wisthaler, A. A Method for Real-Time Detection of PAN, PPN and MPAN in Ambient Air. *Geophys. Res. Lett.* **2000**, *27*, 895–898.
- (50) Blake, R. S.; Monks, P. S.; Ellis, A. M. Proton-Transfer Reaction Mass Spectrometry. *Chem. Rev.* **2009**, *109*, 861–896.